Available online at www.sciencedirect.com
ScienceDirect
Trans. Nonferrous Met. Soc. China 33(2023) 1779−1791
Transactions of Nonferrous Metals Society of China
www.tnmsc.cn

High-temperature oxidation and wear properties of laser cladded Ti−Al−N composite coatings

Yu-xin TIAN, Hua-qiang XIAO, Chuan-chuan YOU, Jin-yu FENG, Yi XIAO, Xuan ZHOU

School of Mechanical Engineering, Guizhou University, Guiyang 550025, China

Received 7 December 2021; accepted 18 April 2022

Abstract: Ti−Al−N composite coatings were in-situ synthesized on TC4 surfaces by laser cladding. The oxidation behaviors and wear properties of the as-obtained composite coatings and TC4 matrix were studied at various temperatures. The results showed the formation of a TiO_2-dominated multilayer film on the composite coating surface at temperatures below 800 °C. The oxidation product of the coating contained a mixed oxide layer of TiO_2 and Al_2O_3 at 900 and 1000 °C. The coatings exhibited good oxidation resistance at high temperatures. The thickening of the oxide film and distribution of the self-lubricating phase Ti_2AlN in the coating decreased the friction coefficient to 0.2091. Also, the wear rate diminished to 0.025×10^{-4} mm^3·N^{-1}·m^{-1} at 800 °C, which is 1.43% that of the TC4 substrate. In the tested temperature range, the composite coatings showed mainly abrasive wear behavior, while an obvious lubrication effect was observed for oxide at high temperatures.

Key words: laser cladding; Ti−Al−N composite coatings; self-lubricating; oxidation; abrasive wear

1 Introduction

Ti−6Al−4V (TC4) is a typical α–β type two-phase titanium alloy that combines the characteristics of α and β type titanium alloys. TC4 is characterized by excellent toughness and thermal stability at low temperatures, and thereby, it is widely used in petrochemical, marine, aerospace, and other load-bearing environments [1−3]. However, the TC4 alloy strongly reacts with oxygen above 550 °C, leading to formation of a weak oxide film with poor protection on its surface [4,5]. In addition, the TC4 alloy has poor wear resistance at high temperatures [6−8], causing serious accidents during long service due to tribological failure. DI et al [9] prepared an AlCoCrFeMoVTi high-entropy alloy coating on the TC4 surface by laser cladding. They noticed the formation of dense oxide films, such as Cr_2O_3 and Al_2O_3 on the cladding layer, which led to significantly improved wear and high-temperature oxidation resistance of TC4. TANG et al [10] obtained a dense modified Zr−N alloying layer using Zr−N ion asynchronous infiltration on TC4. Their results showed significant improvement in the wear resistance of the modified coating, while the wear rate was reduced by 2-fold. Moreover, the coating illustrated good oxidation resistance at high temperatures. Therefore, surface modification technology has been an effective means of enhancing the oxidation resistance, friction, and wear performance of the TC4 alloy at high temperatures.

Compared to traditional ceramic materials, the MAX phase is characterized by a special nanometer lamellar structure and bonding type, leading to excellent properties in terms of the high elastic modulus, high-temperature oxidation resistance, corrosion resistance, and wear resistance [11]. In this respect, ZHANG et al [12,13] prepared a Ti_2AlC coating by supersonic flame spraying and

Corresponding author: Hua-qiang XIAO, Tel: +86-13984168037, E-mail: xhq-314@163.com
DOI: 10.1016/S1003-6326(23)66221-1
1003-6326/© 2023 The Nonferrous Metals Society of China. Published by Elsevier Ltd & Science Press

discharge plasma spraying. The as-obtained coating combined well with the substrate to yield good oxidation resistance and wear resistance. LIU et al [14] prepared a titanium base coating by laser cladding of Ti−TiC−WS_2 on the TA2 alloy. Under the combined effect of the enhanced phase TiC/$(Ti,W)C_{1-x}$ and self-lubricating phase Ti_2SC/TiS, the friction coefficient of the as-obtained coating reached 0.257 at 250 °C, and the wear rate was 0.487×10^{-5} $mm^3\cdot N^{-1}\cdot m^{-1}$ at 500 °C. CAO et al [15] synthesized a Ti_2AlC coating by supersonic flame spraying and studied its high-temperature friction and wear performance. Their data revealed a greatly reduced friction coefficient due to the self-lubricating effect of the coating. SINGH et al [16] and CHEN et al [17] successfully prepared TiC/SiC/Ti_3SiC_2 and SiC/Ti_3SiC_2 composite coatings by spark plasma sintering technology. They then utilized the layered Ti_3SiC_2 phase to improve the high-temperature oxidation and wear properties of the coatings. Previous studies mainly focused on the self-lubricating effect of the MAX phase. However, the oxidation behavior, characterization of oxidation products, and their effects on wear properties should further be clarified, especially for multiphase microstructural composite coatings.

In this work, Ti−Al−N composite coatings were synthesized in-situ by laser cladding. High-temperature cyclic oxidation experiments, as well as high-temperature wear testing, were carried out on the composite coatings. The friction coefficient, wear amount, and microstructure of each composite coating were analyzed on the basis of its oxidation characteristics. The high-temperature wear behaviors and the mechanisms of the composite coatings were investigated to provide support for the preparation of a new composite coating that contains MAX phases on the TC4 surface and its application under high-temperature dynamic load service conditions.

2 Experimental

2.1 Materials and coating preparation

The chemical composition of the TC4 substrate is provided in Table 1. The preparation process consisted of first mixing Ti4822 TiAl powder alloy (purity 99%, 15−53 μm), TiN powder (purity 99%, 2−10 μm), and Al powder (purity 99%, 50−150 μm) at mole ratio of TiAl:TiN:Al=1:1:0.1. A planetary ball mill was used for the mixing followed by drying in a vacuum oven for later use. A YSL−6000 fiber laser system was used for cladding experiments of prefabricated powder coatings under protected argon gas at a flow rate of 10 L/min. The process parameters were set to laser power of 2500 W, scanning speed of 2 mm/s, and spot size of 10 mm × 2 mm. Figure 1 shows the microstructure and XRD pattern of the Ti−Al−N

Table 1 Chemical composition of Ti6Al4V titanium alloy (wt.%)

Al	V	Fe	O	C	N	H	Ti
6.10	4.20	0.30	0.10	0.05	0.015	0.20	Bal.

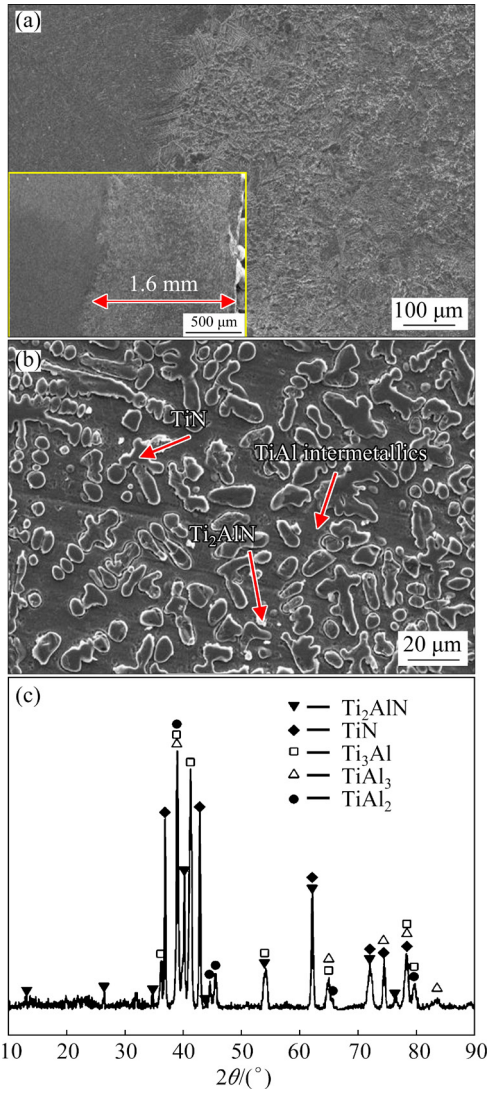

Fig. 1 Microstructures and XRD pattern of Ti−Al−N composite coatings: (a) Interface; (b) High magnification image of middle zone; (c) XRD pattern of as-cladded coating

MAX phase composite coating prepared by laser cladding and the details can be found in our previous work [18]. The coating exhibited a good metallurgical bond with the matrix without the presence of holes, cracks, or other defects. The composite coating was mainly based on TiAl (γ+α_2) phases. The TiN/Ti_2AlN core-shell reinforced phase with dendritic TiN as the core and Ti_2AlN as the shell was formed, and small amounts of equiaxial Ti_2AlN particles were dispersed in the matrix [18].

2.2 Structural characterization and performance evaluation

The microstructure, wear morphology, and high-temperature oxidation morphology of each composite coating were analyzed by field emission scanning electron microscopy (ZEISS Gemini 300). The phase composition of each composite coating was analyzed by a Panaco X'Pert PRO and Bruker X-ray diffractometer.

For oxidation experiments, the TC4 substrate and composite coating samples were first cut into pieces with dimensions of 15 mm × 11 mm × 2 mm. Next, the samples were cyclically oxidized in a SX-6-12 box-type resistance furnace for 50 h at 600, 800, 900 and 1000 °C. An electronic balance with an accuracy of 0.01 mg was employed for weighing the samples. Each experiment was carried out three times, and the average value was obtained. To ensure the accuracy of the oxidation dynamic curves, each sample was weighed at 0.5, 1, 2, 3, and 5 h after beginning the oxidation process, and then it was weighed every 5 h for 50 h.

An UMT-2 system was used for dry sliding wear tests on the TC4 substrate and composite coatings. The test parameters are summarized in Table 2. The size of the wear sample was set to 15 mm × 15 mm × 5 mm, and circular motion wear tests of both the substrate and coating were carried out. The friction matching mode was based on a ball-block type, and the counterpart consisted of a hard Al_2O_3 ball with a diameter of 5 mm. The tests were carried out under an atmospheric environment at 25, 200, 400, 600 and 800 °C. Before testing, the samples were heated in a furnace to the working temperature at a rate of 10 K/min and then kept at the working temperature for 30 min. The test machine system automatically provided the friction coefficient−time curves, in which each friction coefficient was obtained by the average of a series of stable friction coefficients. The wear volume was measured by a three-dimensional profilometer, and the wear rate W_R ($mm^3 \cdot N^{-1} \cdot m^{-1}$) was obtained by a wear quantity corresponding to unit load and sliding distance. The calculations were carried out according to Eq. (1):

$$W_R = \frac{Q}{F \times 2\pi r R t} \tag{1}$$

where Q, F, and r are the wear volume (mm^3), load (N), and wear radius (mm), respectively, R is the revolution speed (r/min), and t is the friction time (min).

After dry sliding wear tests, the worn surface morphologies were analyzed by SEM, and volume loss was measured by a JB-4C surface profilometer.

Table 2 Friction and wear test parameters

Temperature/°C	Load/N	Revolution speed/($r \cdot min^{-1}$)	Wear time/min
25, 200, 400, 600, 800	10	100	20

3 Results and discussion

3.1 High-temperature oxidation behaviors of Ti−Al−N composite coatings

The cyclic oxidation kinetics curves of the TC4 matrix and composite coatings are gathered in Fig. 2. At temperatures from 600 to 800 °C, the mass gain of the Ti−Al−N composite coating looked obviously small after cyclic oxidation for 50 h, ranging from 0.53 to 14.46 mg/cm^2. By comparison, the mass gain of the TC4 substrate under the same conditions varied from 0.85 to 17.47 mg/cm^2. At temperatures from 900 to 1000 °C, the mass gain of the Ti−Al−N composite coating after cyclic oxidation for 50 h ranged from 48.05 to 128.31 mg/cm^2, while that of the TC4 substrate varied from 69.17 to 166.82 mg/cm^2. Thus, the Ti−Al−N composite coatings showed excellent high-temperature oxidation resistance in the temperature range of 600−1000 °C.

As seen from the oxidation kinetics curves, the unit mass gain of composite coatings after cyclic oxidation for 50 h was less than that of the TC4 substrates at every temperature condition. XRD patterns of TC4 substrates and the composite coatings after oxidation are shown in Fig. 3. The oxides of the composite coating were TiO_2 and Al_2O_3; these were the same as those of the TC4

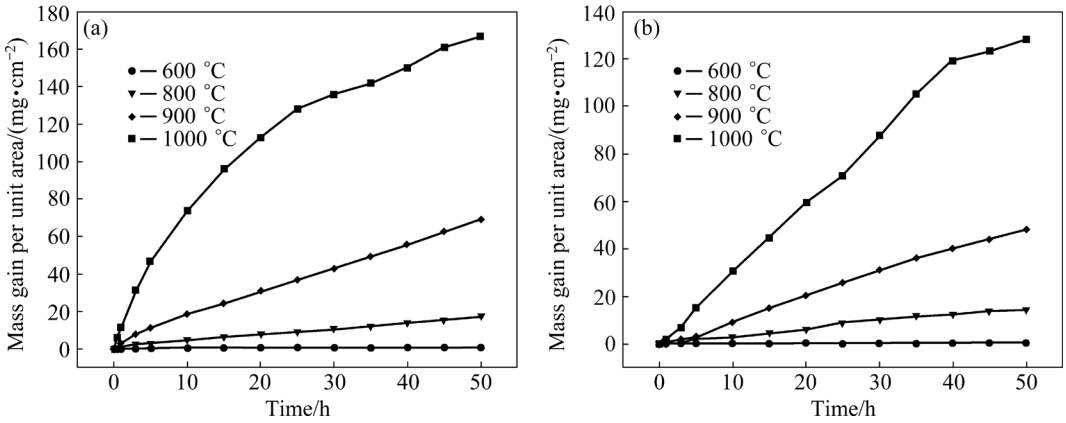

Fig. 2 Oxidation kinetics curves of samples at different temperatures: (a) TC4 alloy; (b) Ti−Al−N composites

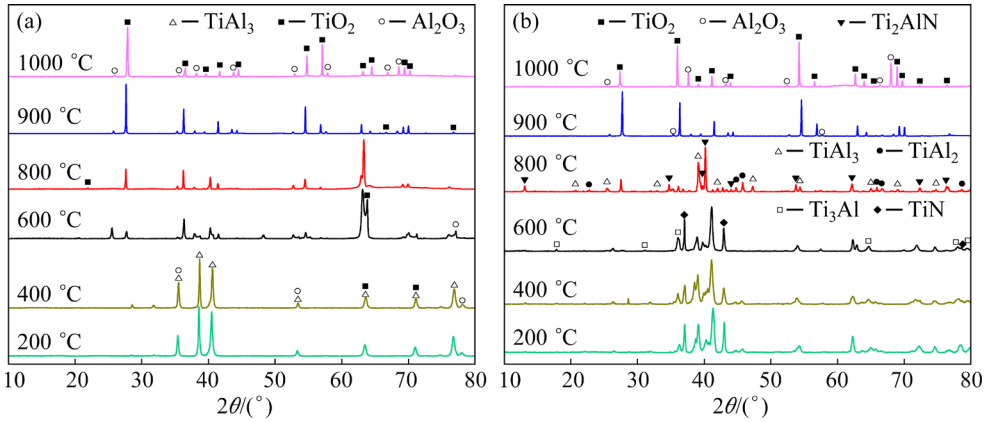

Fig. 3 XRD patterns of TC4 substrates (a) and Ti−Al−N composite coatings (b) after oxidation

substrates, but the amounts of oxides were different. The composition of the coatings before oxidation was mainly Ti_2AlN, TiN, and TiAl intermetallic compounds. The amount of Al atoms in the coatings was much higher than that in the TC4 substrates; this led to a higher content of Al_2O_3 in the oxides of the composite coatings than in the TC4 substrates. It could be inferred that the reason of the mass gain of composite coatings was better than that of the TC4 substrates was mainly related to the formation and content of Al_2O_3. The cross-sectional microstructure and line scan data for the composite coating after oxidation at 1000 °C are shown in Fig. 4. In this condition, the surface oxide of the coating was TiO_2, and the subsurface was Al_2O_3. Previous studies showed similar formation behavior of TiO_2 and Al_2O_3 [19−22]. TiO_2 and Al_2O_3 are generated simultaneously at the start of the oxidation process. However, the Gibbs free energy of Al_2O_3 (which is the product of the Al oxidation reaction) in the early oxidation stage was lower than that of TiO_2 (which is the product of the Ti oxidation reaction). Hence, the growth rate of Al_2O_3

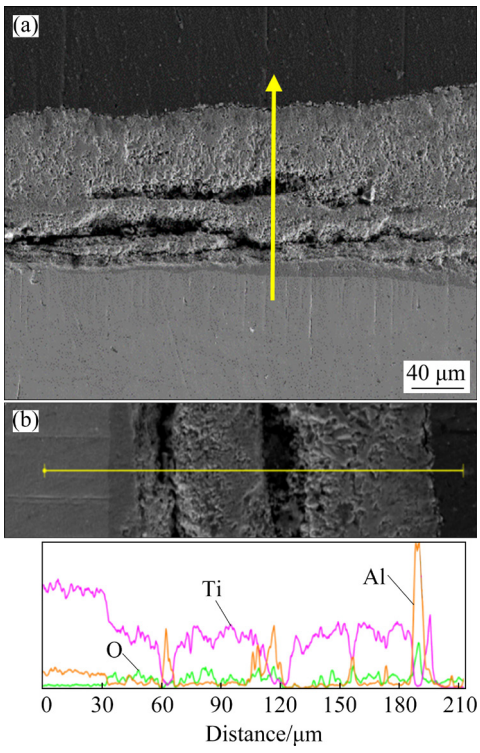

Fig. 4 Cross-sectional microstructure (a) and EDS line scanning results (b) of Ti−Al−N composite coating after oxidation at 1000 °C

was not as fast as that of TiO_2, and a TiO_2 oxide film that was not compact formed on the coating surface. Meanwhile, Al in the coating was enriched near TiO_2 because Ti was consumed. This facilitated the formation of the Al_2O_3 layer. Because of its excellent oxidation resistance, Al_2O_3 can prevent the diffusion of oxygen and metal ions and further inhibit oxidation. However, because of the low content of Al, it was not possible for a compact subsurface layer of Al_2O_3 to form on the TC4 substrate. This resulted in poor high-temperature oxidation resistance of the TC4 substrate compared with composite coating.

The surface morphologies of TC4 substrate after cyclic oxidation for 50 h at different temperatures are provided in Fig. 5. The oxide film began to form on the substrate surface at 200 and 400 °C and looked smooth at 600 and 800 °C with comprehensive oxidation and no cracks. However, the oxide film became uneven after cyclic oxidation at 900 and 1000 °C with some agglomerated oxides. According to the XRD patterns in Fig. 3(a), Al_2O_3 and TiO_2 were both detected in surface oxidation products of the substrate after cyclic oxidation at different temperatures for 50 h. However, the substrate phases were dominated by $TiAl_3$ at 200 and 400 °C, and there was only a small amount of Al_2O_3 and TiO_2. This indicates that there was slight oxidation on the surface of TC4 at those temperatures. At 600 and 800 °C, the surface of the TC4 substrates was covered by oxide films. The $TiAl_3$ phase was not detected in the XRD spectra. Meanwhile, the diffraction peaks of the TiO_2 phase were stronger than those of the Al_2O_3 phase. As a result, TiO_2 oxide film mainly formed during the cyclic oxidation of TC4 at this temperature with

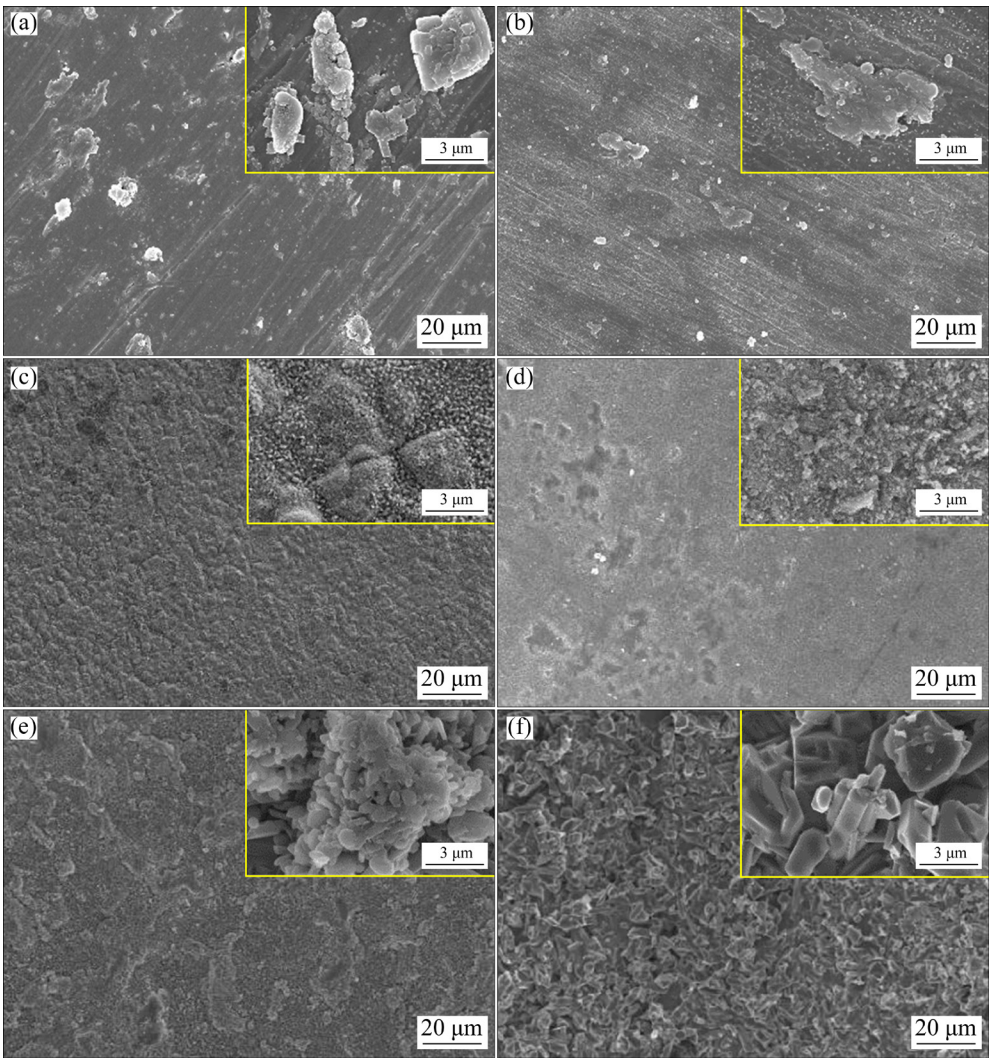

Fig. 5 Surface morphologies of TC4 substrate after cyclic oxidation for 50 h at different temperatures: (a) 200 °C; (b) 400 °C; (c) 600 °C; (d) 800 °C; (e) 900 °C; (f) 1000 °C

small amounts of Al_2O_3. The diffraction peak of the Al_2O_3 phase in the oxidation products at 900−1000 °C gradually increased, indicating an increase in Al_2O_3 products in the oxide layer as a function of temperature.

The micromorphology of oxide films of the composite coatings after cyclic oxidation at different temperatures for 50 h is illustrated in Fig. 6. Comparison between Fig. 5 and Fig. 6 reveals more uniform and compact oxide surface structures of composite coatings than those of the TC4 substrate. Also, no cracks occurred on the oxide surface. No significant oxidation occurred on coatings after cyclic oxidation at 200 and 400 °C for 50 h (Figs. 6(a) and (b)). As seen in Fig. 3(b), the coating phase was mainly composed of Ti_2AlN, TiC, and TiAl intermetallic compounds after oxidation below 600 °C. This indicates that the composite coating only underwent slight oxidation in this temperature range.

After cyclic oxidation at 600 °C for 50 h (Fig. 6(c)), the difference in oxidation performances of all three phases at high temperatures led to an uneven surface due to selective oxidation in local areas. Hence, the oxidation film did not cover the entire surface. The EDS analyses of spectral points in Fig. 6 are summarized in Table 3. At 600 °C, the oxide film on the composite coating surface consisted of the multilayered film that was mainly composed of dendrite TiN at protrusions, a white edge of TiO_2 oxidized from Ti_2AlN particles, and TiO_2 + Al_2O_3 mixed oxide in the relatively flat region. After cyclic oxidation at 800 °C for 50 h (Fig. 6(d)), the oxidation film generated on the composite coating surface became clustered in most areas with some islands in some areas. Also, the oxidation of the coating was more sufficient than that at 600 °C. In Fig. 6(d), the microstructure of the oxidized surface at high magnifications showed a short rod-like phase. Combining XRD (Fig. 3(b))

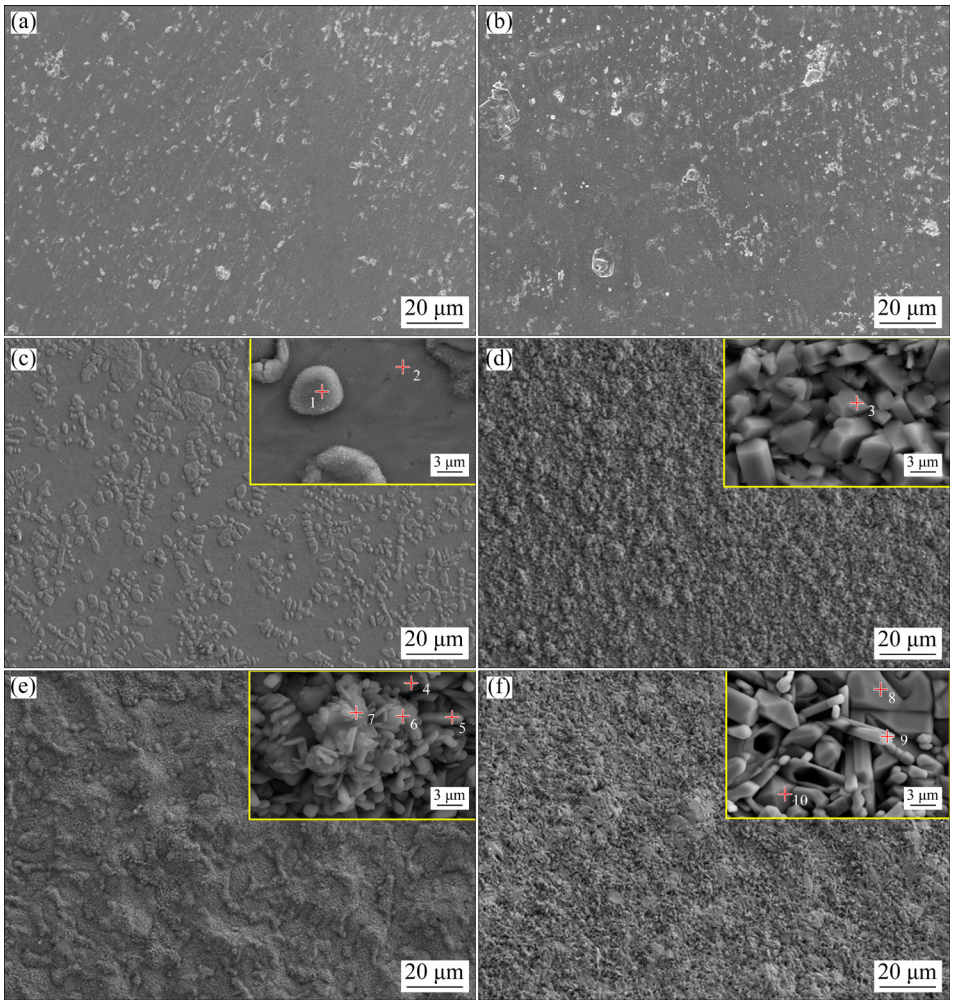

Fig. 6 Surface morphologies of composite coatings after cyclic oxidation for 50 h at different temperatures: (a) 200 °C; (b) 400 °C; (c) 600 °C; (d) 800 °C; (e) 900 °C; (f) 1000 °C

Table 3 EDS results of spectral points shown in Fig. 6 (at.%)

Position	Ti	Al	O	Possible phase
1	34.84	0.62	64.54	TiO_2
2	40.50	19.22	39.78	TiO_2, Al_2O_3
3	26.11	0.18	73.71	TiO_2
4	40.86	6.70	52.44	TiO_2, Al_2O_3
5	25.37	8.20	66.43	TiO_2, Al_2O_3
6	4.06	27.14	68.79	Al_2O_3
7	16.88	13.31	69.81	TiO_2, Al_2O_3
8	34.48	0.70	64.82	TiO_2
9	19.80	1.43	78.77	TiO_2
10	24.05	1.30	74.65	TiO_2

and EDS analyses revealed a slightly higher content of Al_2O_3 than that at 600 °C. Hence, the oxidation product of the composite coating was still mainly TiO_2. After cyclic oxidation at 900 °C for 50 h (Fig. 6(e)), ridges and clusters appeared on the oxidized surface. However, at high magnifications, the oxidized products presented knife-like and granular phases, with small amounts of agglomeration of large lumpy tissue and an uneven oxidized surface. From XRD and EDS data, the small number of coarse granular oxidation product clusters are associated with TiO_2, and the knife-like phase consisted of stable Al_2O_3. Also, the composite coating surface consist of a TiO_2+Al_2O_3 mixed oxide film. The microstructural morphologies of the oxidized composite coating surface after cyclic oxidation at 1000 °C for 50 h are presented in Fig. 6(f). After cyclic oxidation at 1000 °C, the surface of the composite coating was covered with fine oxides, and no pits caused by the difference in oxidation properties were observed. By contrast, more protruding and growing coarse rod-shaped oxide clusters with larger lengths were noticed. In addition, small amounts of knife-chip Al_2O_3 were also visible. From XRD and EDS analyses, the coarse rod-shaped oxide clusters could be related to TiO_2, and oxidation products of the composite coatings consist of mixed oxide layers of TiO_2 and Al_2O_3.

3.2 Wear behaviors of Ti−Al−N composite coatings at different temperatures

The friction coefficient−time curves of the TC4 matrix and Ti−Al−N composite coating at different temperatures are illustrated in Fig. 7. During the initial stage, the contact area between the friction pair and composite coating changed to a plane. This process expanded the contact surface and increased the frictional shear force. This resulted in transient fluctuations of the friction coefficient curves of TC4 and the composite coating at different temperatures [23,24]. After a period of wear, the dynamic friction coefficient curves had relatively stable trends. The steady-state friction coefficients of composite coatings at 25, 200, 400, 600, and 800 °C were estimated to be 0.4036, 0.3358, 0.3406, 0.2695, and 0.2091, respectively. The friction coefficients of the coatings decreased gradually at high temperatures because of softening of the coatings as the temperature rose. Here, the actual temperature of the contact surface was higher due to the friction between the composite coating and Al_2O_3 counterpart. At higher temperature, the diffusion of oxygen intensified, resulting in accelerated rates of oxide formation on the composite coating surface to yield denser and thicker oxide films. The presence of fine oxide debris can also prevent direct contact between the

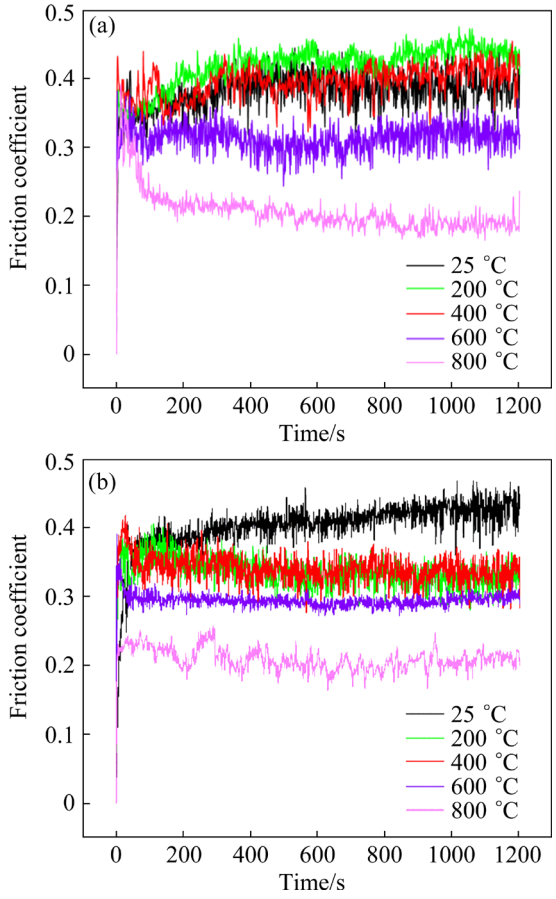

Fig. 7 Friction coefficient−time curves of TC4 substrate (a) and composite coating (b) at different temperatures

coating and counterpart, further reducing the friction coefficient. Therefore, oxide films formed at high temperatures possessed certain self-lubricating effects on the friction of the coating.

Figure 8 compares the steady-state friction coefficients and wear rates of TC4 and composite coatings at different temperatures. The friction coefficients of the coatings at 200, 400, and 600 °C were lower than those of the substrate (Fig. 8(a)). At 25 °C, the reciprocating change in the load stress led to direct contact between the reinforcement particles on the coating surface and Al_2O_3 counterpart, resulting in fatigue failure. The particles then fell off to become abrasive particles, leading to three-body wear behavior. Consequently, the friction coefficient of the coating was slightly higher than that of TC4 substrate. At 800 °C, the friction coefficient of the TC4 decreased to reach that of the softened coating of TC4.

As shown in Fig. 8(b), the wear rate of the TC4 substrate showed an overall downward trend below 600 °C. However, the TC4 substrate was exfoliated during the wear process at 800 °C because of the local adhesive wear, and this resulted in a significant increase in the wear rate. The wear rate of the composite coating decreased rapidly as the temperature increased, especially at 400 °C. Combined with the oxidation morphology, it can be concluded that the oxide film formed at higher temperatures isolated the contact surface. Also, the contact between the Al_2O_3 counterpart with the composite coating induced shear slipping of the Ti_2AlN self-lubricating phase distributed in the coating under stress during friction. This achieved a better lubrication effect and effectively reduced the wear rate of the composite coating [21]. As a result, the wear rates of composite coatings were lower than those of the substrate at high temperatures.

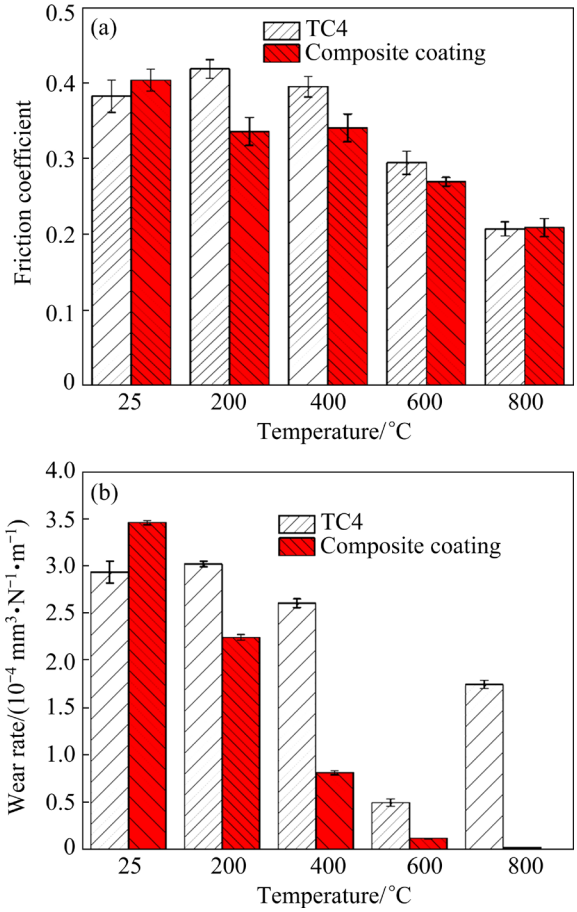

Fig. 8 Friction and wear properties of TC4 and composite coating at different temperatures: (a) Steady-state friction coefficient; (b) Wear rate

At 800 °C, the wear rate of the TC4 substrate was estimated to be 1.748×10^{-4} $mm^3\cdot N^{-1}\cdot m^{-1}$, while that of the composite coating was only 0.025×10^{-4} $mm^3\cdot N^{-1}\cdot m^{-1}$ (1.43% that of TC4 substrate). The reason for this had to do with the temperature increase, which enhanced the thickness and formation rate of the oxide film. Also, the fine oxide particles that were present on the composite coating surface played an excellent lubrication role, further declining the wear of the composite coating. Meanwhile, the local plastic flow of the oxide layer at high temperatures further reduced the friction coefficient and wear rate of the coating. Consequently, the coatings showed better wear resistance at high temperatures than TC4 did.

3.3 Wear mechanism of Ti−Al−N composite coatings at high temperatures

SEM images showing wear morphologies of the TC4 substrate at different temperatures are depicted in Fig. 9. Serious abrasive wear occurred on the TC4 surface at low temperatures. The hardness of the Al_2O_3 pair was much higher than that of TC4, and a normal load facilitated pressing of the friction pair into the surface. Under the action of continuous frictional shear stress, continuous shear wear and fatigue wear took place on the surface, leaving a relatively obvious furrow. Under the ploughing action of the hard friction pair, the substrate surface was peeled off. Some spalling material gradually broke away from the wear scar with the progress of wear, while some broke under the action of friction stress to form fine debris particles. This formed three-body wear between the

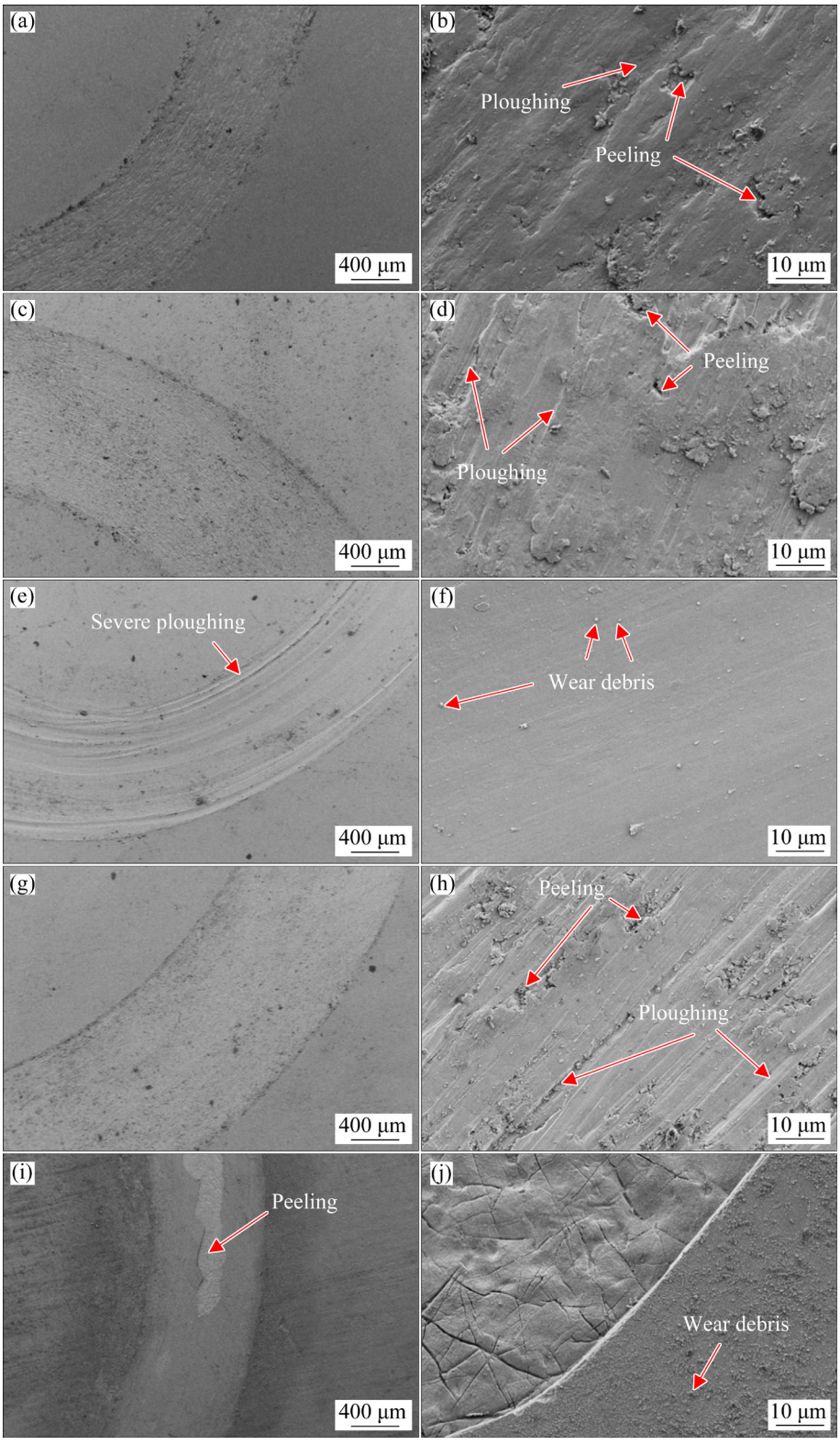

Fig. 9 Wear scar morphologies of TC4 titanium alloy substrate at different temperatures: (a, b) 25 °C; (c, d) 200 °C; (e, f) 400 °C; (g, h) 600 °C; (i, j) 800 °C

friction pairs [25]. At 600 °C or above, the abrasive wear on the substrate surface reduced. At 800 °C, the matrix oxide TiO_2 grew rapidly and protruded from the surface of the substrate. It broken and peeled off under the fatigue effect between the friction pairs, and this also led to an increase in the wear rate of the TC4 substrate.

The wear morphologies of Ti−Al−N composite

coatings at different temperatures are shown in Fig. 10. At room temperature, the alternating stress between the wear pairs separated a small number of reinforced particles from the substrate and fatigue failure occurred (Figs. 10(a) and (b)). This resulted in large numbers of tortoise cracks on the coating surface. As the temperature rose to 400 °C, large numbers of pits and chips formed on the surface of

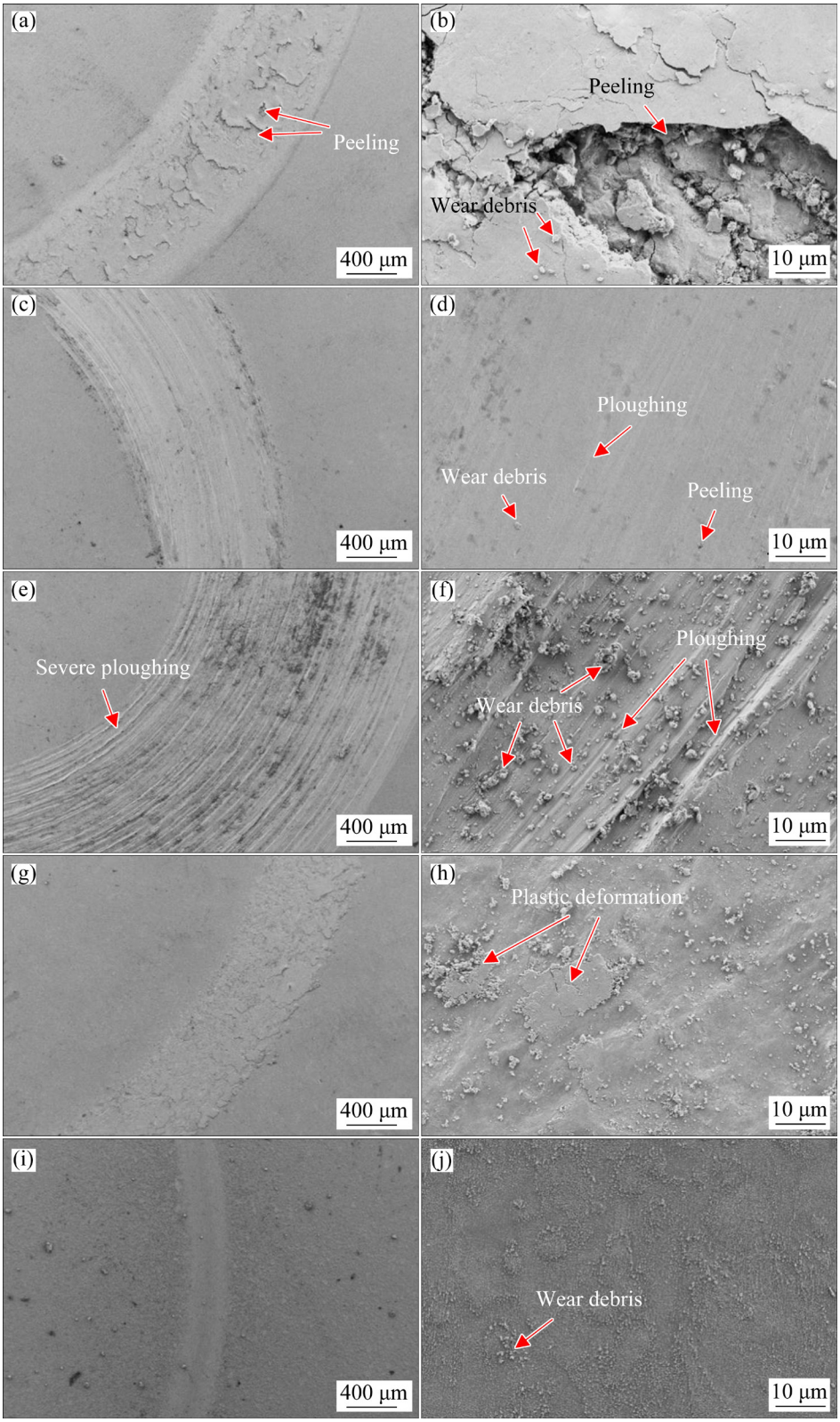

Fig. 10 Wear scar morphologies of composite coatings at different temperatures: (a, b) 25 °C; (c, d) 200 °C; (e, f) 400 °C; (g, h) 600 °C; (i, j) 800 °C

the coating wear scars (Figs. 10(e) and (f)). Hence, TiO_2-based oxide film on the coating surface played a certain role in lubrication and protection. However, insufficient oxidation on the coating surface at lower temperatures led to ineffective protection of the material. The oxide film that continuously formed on the coating surface broke and peeled off. In turn, the peeled oxide particles acted as abrasive particles to form three-body abrasive wear, aggravating the loss of materials [25]. In Figs. 10(g) and (h), a further increase in temperature to 600 °C accelerated the formation rate of oxide on the composite coating surface to yield a denser film. Also, the oxide film dominated by TiO_2 became thick. The fine oxide debris played a good lubrication role, further reducing the volume loss of composite coating. Meanwhile, the frictional heat effect caused by high-temperature friction and wear led to local plastic flow of the oxide layer, further decreasing the friction coefficient of coating and the wear amount of the material. At 800 °C (Figs. 10(i) and (j)), the oxidation products of the composite coating increased, and the structure became uniform and compact. Also, the coating became strongly bonded to the oxide film, thereby reducing the friction effect between the coating and wear pair.

The three-dimensional morphologies of wear scars of composite coating wear samples are provided in Fig. 11. The cross-section areas of wear scars of the composite coatings decreased gradually at 25, 200, 400, 600, and 800 °C. As shown in Fig. 11(a), the wear scars at room temperature mainly consisted of furrow scars produced by abrasive wear with cross-section area estimated to be 6.882×10^{-3} mm^2. The large amounts of the TiN hard phase in the Ti−Al−N composite coating greatly improved the microhardness of the coating, and the adhesion between the friction coupling component and composite coating surface reduced. However, the uneven distribution of the hard phase led to serious abrasive wear on the surface, and the surface of wear scars showed signs of crushing. According to Figs. 11(d) and (e), the cross-sectional area of the composite coating decreased to 0.250×10^{-3} mm^2 at 600 °C and 0.053×10^{-3} mm^2 at 800 °C. The surface of the wear scar looked smooth and the abrasive chip declined. These results were significantly different from those at 400 °C, indicating enhanced isolation and lubrication of the oxide film with thickening of the oxide film.

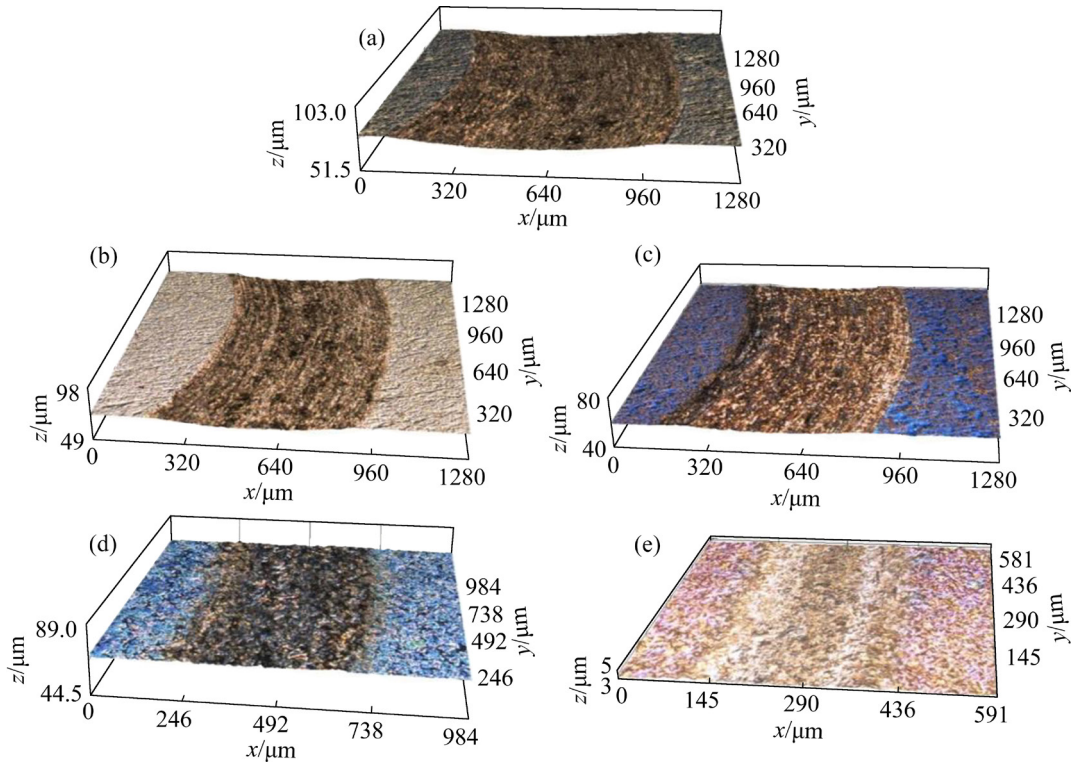

Fig. 11 Three-dimensional wear scar morphologies of composite coatings at different temperatures: (a) 25 °C; (b) 200 °C; (c) 400 °C; (d) 600 °C; (e) 800 °C

4 Conclusions

(1) The oxidation mass gain of the TC4 substrate at 1000 °C was estimated to be 166.82 mg/cm^2, while the oxidation mass gain of the Ti−Al−N composite coating was 128.31 mg/cm^2, which is 76.9% that of the substrate. Compare to the TC4 substrate, the oxidation resistance of the coating increased because of an obvious increase in the content of Al_2O_3 in the oxidation layer.

(2) At high temperatures, the friction coefficients and wear rates of the Ti−Al−N composite coatings declined gradually as temperature increased. The friction coefficient of the Ti−Al−N composite coating decreased to 0.2091 at 800 °C, and the wear rate was estimated to be 0.025×10^{-4} mm$^3\cdot$N$^{-1}\cdot$m^{-1}, which is only 1.43% that of TC4.

(3) The composite coatings showed mainly abrasive wear behavior at the investigated temperature. As temperature rose, the thickened oxide layer gradually isolated the friction pairs, as well as played a role in self-lubrication and resistance to indentation of the friction pairs.

Acknowledgments

The authors are grateful for the financial supports from the National Natural Science Foundation of China (No. 52065009), the Science and Technology Planning Project of Guizhou Province, China (No. ZK2021269), and the Science and Technology Planning Project of Guiyang, China (No. 2021.1-4).

References

[1] CARROLL B E, PALMER T A, BEESE A M. Anisotropic tensile behavior of Ti−6Al−4V components fabricated with directed energy deposition additive manufacturing [J]. Acta Materialia, 2015, 87: 309−320.

[2] YANG Xin, WANG Wan-lin, MA Wen-Jun, WANG Yan, YANG Jun-gang, LIU Shi-feng, TANG Hui-ping. Corrosion and wear properties of micro-arc oxidation treated Ti−6Al−4V alloy prepared by selective electron beam melting [J]. Transactions of Nonferrous Metals Society of China, 2020, 30(8): 2132−2142.

[3] SUN Hong, YU Li-ming, LIU Yong-chang, ZHANG Li-ye, LIU Chen-xi, LI Hui-jun, WU Jie-feng. Effect of heat treatment processing on microstructure and tensile properties of Ti−6Al−4V−10Nb alloy [J]. Transactions of Nonferrous Metals Society of China, 2019, 29(1): 59−66.

[4] DONG En-tao, YU Wei, CAI Qing-wu, CHENG Lei, SHI Jia-xin. High- temperature oxidation kinetics and behavior of Ti−6Al−4V alloy [J]. Oxidation of Metals, 2017, 88: 719−732.

[5] GULERYUZ H, CIMENOGLU H. Oxidation of Ti−6Al−4V alloy [J]. Journal of Alloys and Compounds, 2009, 472(1/2): 241−246.

[6] ZHANG Jin-hu, LI Xue-yong, XU Dong-sheng, YANG Rui. Recent progress in the simulation of microstructure evolution in titanium alloys [J]. Progress in Natural Science: Materials International, 2019, 29(3): 295−304.

[7] CAO Lei, LIU Jian, WAN Yong, YANG Shu-yan, GAO Jian-guo, PU Ji-bing. Low-friction carbon-based tribofilm from poly-alpha-olefin oil on thermally oxidized Ti−6Al−4V [J]. Surface and Coatings Technology, 2018, 337: 471−477.

[8] GANGWAR K, RAMULU M. Friction stir welding of titanium alloys: A review [J]. Materials & Design, 2018, 141: 230−255.

[9] DI Ying-nan, LIU Hong-xi, ZHANG Xiao-wei, CHEN Lin, LIU Jing-zhou, LIN Jian-quan, HAO Xuan-hong, WANG Yue-yi. Friction and wear behavior and high-temperature oxidation resistance of laser cladding AlCoCrFeMoVTi high-entropy alloy coating on titanium alloy surface [J]. Rare Metal Materials and Engineering, 2021, 50(08): 2883−2891. (in Chinese)

[10] TANG Jin-gang, LIU Dao-xin, TANG Chang-bin, YU Shou-ming, ZHANG Xiao-hua. Tribology behavior of Zr−N alloying layer on Ti6Al4V alloy surface at elevated temperature [J]. Rare Metal Materials and Engineering, 2013, 42 (2): 331−335. (in Chinese)

[11] JAMSHIDI R, BAYAT O, HEIDARPOUR A. Tribological and corrosion behavior of flame sprayed Al−10wt.% Ti_3SiC_2 composite coating on carbon steel [J]. Surface and Coatings Technology, 2019, 358: 1−10.

[12] ZHANG Z, LIM S H, CHAI J W, LAI D M Y, LIM P C, CHEONG A K H, WANG S J, JIN H M, PAN J S. Kerosene-fuelled high velocity oxy-fuel (HVOF) spray of Ti_2AlC MAX phase powders [J]. Journal of Alloys and Compounds, 2018, 735: 377−385.

[13] ZHANG Z, LAI D M Y, LIM S H, CHAI J W, WANG S J, JIN H M, PAN J S. Isothermal oxidation of the Ti_2AlC MAX phase coatings deposited by kerosene-fuelled HVOF spray [J]. Corrosion Science, 2018, 138: 266−274.

[14] LIU Xiu-bo, WANG Mian, QIAO Shi-jie, ZHAI Yong-jie, ZHOU Zhong-yan, LUO Ying-she, TU Rong. High temperature tribological properties of laser cladding titanium matrix self-lubricating wear resistant composite coating on TA2 alloy [J]. Tribology, 2018, 38(3): 283−290. (in Chinese)

[15] CAO Jun, YIN Zhong-wei, LI Hu-lin, GAO Gen-yuan, ZHANG Xiu-li. Tribological and mechanical properties of Ti_2AlC coating at room temperature and 800 °C [J]. Ceramics International, 2018, 44(1): 1046−1051.

[16] SINGH A, BAKSHI S R, VIRZI D A, KESHRI A K, AGARWAL A, HARIMKAR S P. In-situ synthesis of TiC/SiC/Ti_3SiC_2 composite coatings by spark plasma sintering [J]. Surface and Coatings Technology, 2011, 205(13/14): 3840−3846.

[17] CHEN Ding, GU Hua-zhi, HUANG Ao, NI Hong-wei. Mechanical performance and oxidation resistance of SiC

castables with lamellar Ti_3SiC_2 coatings on SiC aggregates prepared by SPS [J]. Journal of Alloys and Compounds, 2019, 791: 461−468.

[18] YOU Chuan-chuan, XIAO Hua-qiang, REN Li-rong, ZHAO Xin-xin. Microstructure and properties of laser cladding Ti−Al−N composite coating on TC4 surface [J]. Laser Technology, 2021, 45(5): 585−589. (in Chinese)

[19] ZHAO Kun, OUYANG Si-hui, LIU Yong, LIU Bin, LIANG Xiao-peng, LI Hui-zhong, WANG Yu. Isothermal oxidation behavior of TiAl intermetallics with different oxygen contents [J]. Transactions of Nonferrous Metals Society of China, 2019, 29(3): 526−533.

[20] PAN Yu, LU Xin, HUI Tai-long, LIU Cheng-cheng, LIU Bo-wen, XU Wei, ZHANG Ce, SUN Jian-zhou, QU Xuan-hui, ZHANG Jia-zhen. High-temperature oxidation behaviour of TiAl alloys with Co addition [J]. Journal of Materials Science, 2021, 56(1): 815−827.

[21] MALIUTINA I N, MOHAND H S, PIOLET R, MISSEMER F, POPELYUKH A I, BELOUSOVA N S, BERTRAND P. Laser cladding of γ-TiAl intermetallic alloy on titanium alloy substrates [J]. Metallurgical and Materials Transactions A, 2016, 47: 378−387.

[22] WEI Dong-bo, ZHANG Ping-ze, YAN Yu-qin, CHEN Xiao-hu, LI Feng-kun, WANG Shi-yuan, YAO Zheng-jun. High-temperature oxidation of double-glow plasma tantalum alloying on γ-TiAl [J]. Oxidation of Metals, 2019, 92(3/4): 337−351.

[23] WANG Da-qun, SUN Dong-li, HAN Xiu-li, WANG Qing, ZHANG Ning-bo. Investigation on tribological behavior of Ti_2AlN/TiAl composite at room and elevated temperature [J]. Tribology Letters, 2018, 66(2): 52.

[24] CAI Chao, SONG Bo, QIU Chun-lei, LI Li-fan, XUE Peng-ju, WEI Qing-song, ZHOU Jian-xin, NAN Hai, CHEN Hong-xia, SHI Yu-sheng. Hot isostatic pressing of in-situ TiB/Ti−6Al−4V composites with novel reinforcement architecture, enhanced hardness and elevated tribological properties [J]. Journal of Alloys and Compounds, 2017, 710: 364−374.

[25] XIAO Hua-qiang, CHEN Yu-jia, CHEN Wei-ping. HE Jia-rong, ZHAO Si-hao. Research progress on corrosion-wear behavior of materials in molten aluminum [J]. Materials Reports, 2020, 34(7): 123−129. (in Chinese)

激光熔覆 Ti−Al−N 复合涂层高温氧化及摩擦磨损性能

田雨鑫，肖华强，游川川，冯进宇，肖 易，周 璇

贵州大学 机械工程学院，贵阳 550025

摘 要：采用激光熔覆于 TC4 合金表面原位合成 Ti−Al−N 复合涂层，对比研究复合涂层及 TC4 基体的高温氧化行为及宽温域下的摩擦磨损性能。结果表明：复合涂层在 800 ℃以下生成以 TiO_2 为主的多层膜，在 900 和 1000 ℃下涂层氧化产物为 TiO_2 和 Al_2O_3 的混合氧化层，涂层表现出较好的抗高温氧化性能；由于氧化膜增厚及涂层中分布的 Ti_2AlN 自润滑相的作用，800 ℃时涂层摩擦因数降至 0.2091，磨损率降至 0.025×10^{-4} $mm^3\cdot N^{-1}\cdot m^{-1}$，是 TC4 钛合金基体的 1.43%。复合涂层在测试温度区间以磨粒磨损为主，高温条件下氧化物具有明显的润滑作用。

关键词：激光熔覆；Ti−Al−N 复合涂层；自润滑；氧化；磨粒磨损

(Edited by Xiang-qun LI)